Neurocomputing 175 (2016) 25–39

Contents lists available at ScienceDirect

Neurocomputing

journal homepage: www.elsevier.com/locate/neucom

Single satellite image dehazing via linear intensity transformation and local property analysis

Weiping Ni, Xinbo Gao *, Ying Wang

School of Electronic Engineering, Xidian University, Xi'an 710071, China

ARTICLE INFO

Article history:
Received 22 April 2015
Received in revised form
12 August 2015
Accepted 6 October 2015
Communicated by: Jungong Han
Available online 29 October 2015

Keywords:
Single satellite image
Dehaze
Linear intensity transforming
Local property analysis

ABSTRACT

Contrast enhancement of hazy image, or known as image dehazing has always been a practical and challenging topic in image processing and analysis field. Quite a number of strategies have been proposed to determine the depth information, which reflects the thickness of haze over the captured natural images. However, as for remote sensing imagery, too high satellite orbit makes the depth information meaningless. Most of the existing physical-model based methods of natural images fail to enhance the contrast of satellite imagery. In this paper, we present a simple but effective method to remove the haze from single satellite image. This method is developed with the linear intensity transformation (LIT) and local property analysis (LPA). Considering the difference between impacts of depth information on hazy natural image and hazy satellite image, we firstly employ classical degradation model to demonstrate the rationality of utilizing LIT to enhance the visibility of hazy satellite imagery. And then, we propose to adaptively estimate parameters of LIT by analyzing the local image properties of luminance, chromatics and texture. Experimental results on hazy satellite imagery, *obtained from Google Earth and NASA Earth Observatory websites,* illustrate that compared with state-of-the-arts, the proposed method can more efficiently and effectively on enhancing the overall contrast of hazy satellite imagery.

1. Introduction

Owing to their high spatial resolution, optical satellite imageries acquired, (e.g., by *SPOT-5, Quickbird-2, Pleiades-1, World-view-2, and GeoEye-1*), have increased the possibility of accurate observations of Earth [1]. They have been widely used for scene analysis [2], precision agriculture [3], city planning [4], and land surveillance [5,6]. The existence of haze often seriously decreases image contrast in terms of poor content visibility, bad detail perceptibility and heavy color saturation. Fig. 1 shows two examples of hazy satellite images. It can be seen that the useful information in such images has been greatly reduced. Since necessary and appropriate contrast is of great importance for many applications to extract image features from a collection of satellite imagery, how to enhance the contrast of hazy satellite imagery has already been one urgent research topic [7].

In the past decades, several methods, including histogram equalization (HE) [8] and intensity transformation (IT) [9], have been developed to enhance image contrast. However, for HE-based methods, they restore images with uniformly distributed histograms by spreading out those values that occur more frequently and compressing those values that occur less frequently. The gray levels cannot be well maintained, resulting in either under- or oversaturation in the processed image. For the IT-based methods, they strongly depend on prior knowledge of image degradation model. To avoid these problems, many substitute methods have been developed.

Some methods, including the well-known homographic filter (HF) and Retinex theory, have been proposed based on the assumption that a hazy image is the product of illumination and reflectance [10]. These methods commonly extract reflectance by removing the illumination. Since the illumination, actually necessary to represent ambience, is impossible to precisely remove, these methods often fail to present satisfying results. For satellite imagery, the haze optimized transformation (HOT) was proposed to detect and remove the haze under the condition that the blue and red bands are highly correlated [11]. However, this correlation does not always hold, and the results strongly depend on the pre-selection of haze-free regions.

Recently, some other methods, benefiting from the significant progresses in natural image dehazing, have also been developed [12–16]. For these methods, the Koschmieder's law-based model is often used to describe the degradation procedure of haze image. Fattal proposed to dehaze natural images under the assumption that surface shading and transmission are locally uncorrelated [14]. This method is physically reasonable, but it is invalid to handle heavily hazed regions. Tan et al. [15]

* Corresponding author.

http://dx.doi.org/10.1016/j.neucom.2015.10.010
0925-2312/

Fig. 1. Example of hazy satellite images. As can be seen that poor contrast makes target detection and image interpretation difficult.

dehazed images by maximizing the local contrast of the restored image. Due to the possible overestimated haze concentration, his results showed more visibility for dense haze regions, but tended to be over-saturated for haze-free regions. The results may not be physically valid. He et al. [16] proposed to dehaze the natural images using the dark channel prior (DCP) method on high cost of calculation. Although, it is currently one of the most effective dehazing methods, it may be invalid when the scene object is inherently close to the airlight. Meng et al. [17] sped up DCP with boundary constraints and contextual regularization (BCCR-DCP). Long et al. [18] directly conducted DCP on hazy satellite images. For the difference of imaging mode between satellite sensors (downward-looking) and outdoor cameras (forward-looking), the lack of relative depth variation of downward-looking at high orbit, actually destroys the foundation of DCP-based dehazing for satellite images. Accordingly, local properties and priors have been used to enhance the contrast of hazy images [19–22]. Huang. et al. [23] proposed to remove haze from single image using the change of detail prior. Lee et al. [24] utilized brightness analysis and adaptive intensity transformation to enhance contrast in satellite images. Tarel et al. [25] presented to enhance the visibility of outdoor images with prior scene. Besides contrast enhancement, most existing methods suffer from color saturation, detail distortions and complicated calculations.

In this paper, we propose a novel method to dehaze single satellite image using linear intensity transformation (LIT) and local property analysis (LPA). Based on the analysis about degradation model of hazy satellite image and the observations of the intensity distribution of each RGB color channel, we demonstrate the rationality of LIT for hazy satellite image. Then LPA, which is concerned with localized luminance, chromatic nature and texture, is used to estimate the LIT parameters. Finally, with images obtained from *Google Earth and NASA Earth Observatory websites*, the performance of our method was evaluated by comparison with other methods, including the classical and state-of-the-arts.

This paper is organized as follows. In Section 2, the appropriateness of LIT to dehaze single hazy satellite image is discussed. Section 3 presents parameter estimations for LIT via LPA. The experimental results and comparisons with other methods are given in Section 4. Finally, conclusions are drawn in Section 5.

2. Rationality demonstration of linear intensity transformation for hazy satellite image

2.1. Physical model of hazy image

According to Koschmieder's law [8], the model widely used in computer vision and computer graphics to describe the formation of a hazy image is

$$\mathbf{I}(\mathbf{x}) = \mathbf{J}(\mathbf{x})t(\mathbf{x}) + \mathbf{A}[1 - t(\mathbf{x})], \tag{1}$$

where $\mathbf{x}$ is a two-dimensional (2D) spatial location, $\mathbf{I}(\mathbf{x})$ is the observed image, $\mathbf{J}(\mathbf{x})$ is scene radiance, $\mathbf{A}$ is global atmospheric light, and $t(\mathbf{x})$ is transmission associated with not only the scattering of atmosphere, but also the distances between observed scene and imaging sensors. Enhancing the contrast of hazy image is actually to recover $\mathbf{J}(\mathbf{x})$ from $\mathbf{I}(\mathbf{x})$.

In Eq. (1), the first term $\mathbf{J}(\mathbf{x})t(\mathbf{x})$ on the right-hand side is the *direct attention* related to the media transmission coefficient. It describes the scene radiance, and diminishes with $t(\mathbf{x})$. The second term $\mathbf{A}[1-t(\mathbf{x})]$ is called the *airlight*. It increases as $t(\mathbf{x})$ decreases. The main reason for the reduction of image quality is that the scene radiance is depleted by haze and far-away objects.

2.2. Linear intensity transformation

If the haze is homogenous, $t(\mathbf{x})$ can be estimated as

$$t(\mathbf{x}) = e^{-\beta d(x)}, \tag{2}$$

where β is the medium extinction coefficient, and $d(\mathbf{x})$ is the scene depth related with the distance between object and camera. For natural image, $d(\mathbf{x})$ is of importance for $t(\mathbf{x})$, whereas for satellite image, considering the high orbit in space, the distances between objects in a given scene and the imaging sensor are approximately changeless. Thus, $t(\mathbf{x})$ mainly depends on the characteristics of atmosphere or haze. Since the haze over a small local region is usually homogenous, $t(\mathbf{x})$ can be noted as a constant t_0:

$$\mathbf{I}(\mathbf{x}) = \mathbf{J}(\mathbf{x})t_0 + \mathbf{A}[1 - t_0], \tag{3}$$

Obviously, the observed image formally consists of two parts: the desirable scene image transmitted through haze and the undesirable haze overcastting. The former could reduce the dynamic range of image intensity, and the latter may change the image intensity into high values. For dense haze, the low transmission results in that the *airlight* term nears to the highly-valued global atmospheric light. Meanwhile, the dynamic range of

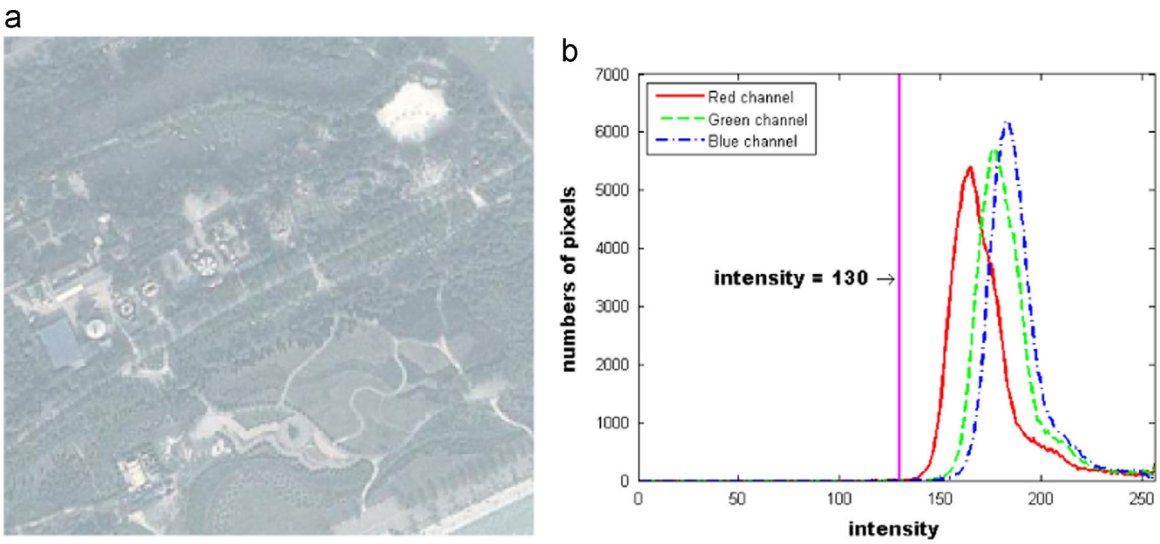

Fig. 2. Hazy satellite image and its intensity distribution: (a) shows a hazy satellite image; (b) illustrates the intensity histograms of RGB channels for (a).

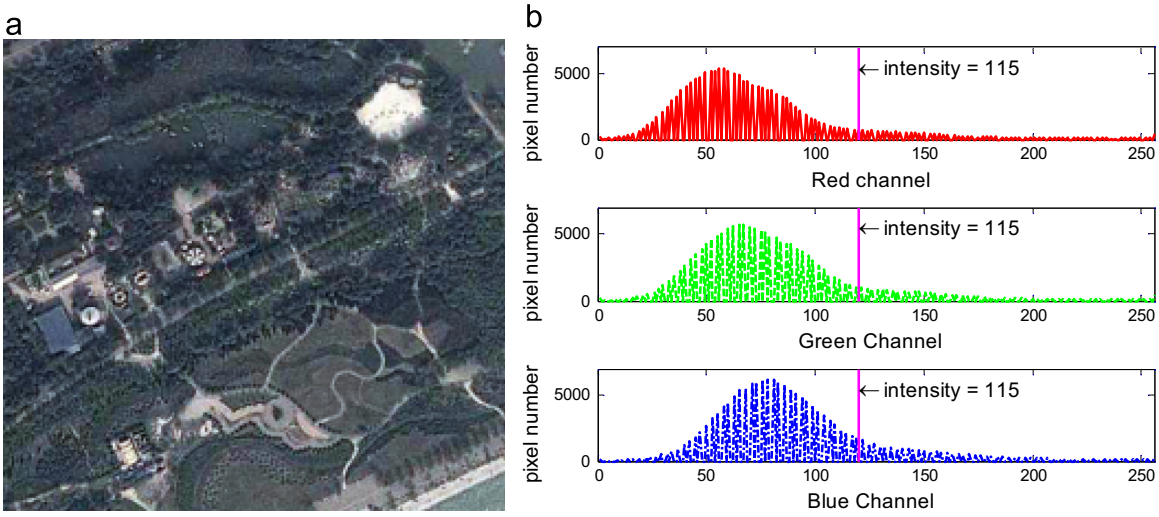

Fig. 3. Dehazing result with simple LIT method: (a) Contrast enhancement via LIT; and (b) color intensity histograms for enhanced image with RGB channel. (For interpretation of the references to color in this figure legend, the reader is referred to the web version of this article)

intensities is shortened for all RGB color channels. Fig. 2 shows a hazy satellite image with histograms of each RGB color channel. Note that most RGB color intensities are larger than 130. The main range of color intensities for each channel spans just about 50. This phenomenon is consistent with Eq. (3), and destroys the assumptions of DCP-based method.

Rewrite Eq. (3), and let k denote $1/t_0$ and b denote $\mathbf{A}(1-t_0)/t_0$, then we obtain

$$\mathbf{J}(\mathbf{x}) = k\mathbf{I}(\mathbf{x}) - b \quad ; \quad k \geq 1 \; ; \; b \geq 0, \tag{4}$$

This is a typical expression of LIT for image contrast enhancement. Fig. 3 shows the result of LIT for Fig. 2(a). We can find that the haze is removed well by LIT alone. It further validates the rationality of LIT for haze satellite image. However, the processed image still suffers from low visibility (mainly lower than 115), especially in those regions with dense haze and low light conditions. Therefore, the image has not been sufficiently enhanced.

According to the analysis presented above, it can be concluded that the local contrast of hazy satellite image depends on local haze characteristics instead of local scene depth information. To obtain better dehazing effects, we should employ localized spatial properties of haze to adaptively estimate parameters $k(\mathbf{x})$ and $b(\boldsymbol{x})$.

3. Estimate the parameters of linear intensity transformation via local property analysis

This section focuses on the method how to estimate the parameters $k(\mathbf{x})$ and $b(\boldsymbol{x})$ defined in Section 2. In the first part, LPA is proposed to estimate parameter $k(\mathbf{x})$, and then parameter $b(\mathbf{x})$ is estimated accordingly.

3.1. Estimate parameter $k(\mathbf{x})$

As defined above, we have $k(\mathbf{x}) = 1/t(\mathbf{x})$. Therefore, parameter $k(\mathbf{x})$ can be calculated with parameter $t(\mathbf{x})$. It denotes the modulation of haze on scene reflectance. Since the haze over a scene is not thoroughly homogenous, $t(\mathbf{x})$ often varies with the localized properties of haze. This means that dense haze usually results in a smaller $t(\mathbf{x})$ than light haze. Motivated by such phenomena, we use local property analysis, denoted as LPA, to adaptively estimate t.

For the convenience of calculation, the hazy satellite image is normalized beforehand

$$\mathbf{I}_n(\mathbf{x}) = \mathbf{I}(\mathbf{x})/255, \tag{5}$$

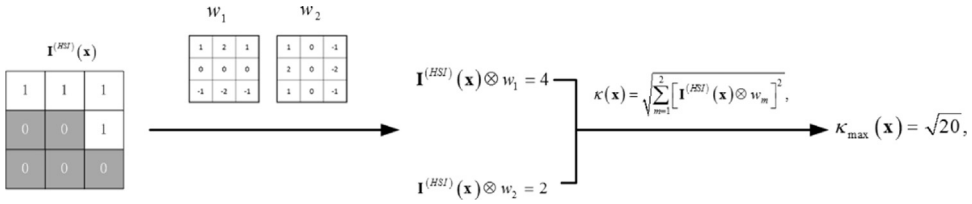

Fig. 4. Flowchart of how the maximum value of κ_{max} is calculated.

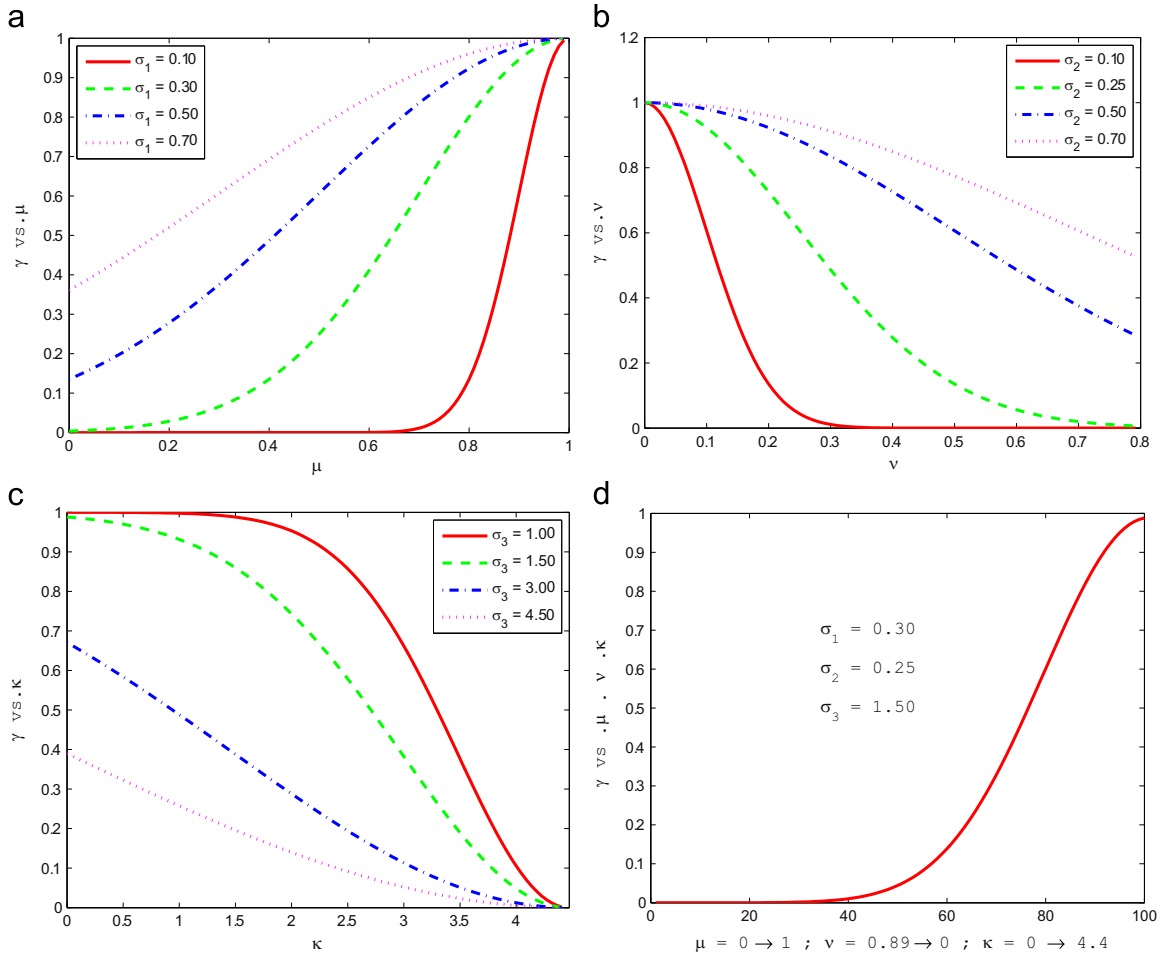

Fig. 5. Change curves of $\gamma(\mathbf{x})$ with different factors: (a) curves of $\gamma(\mathbf{x})$ vs. $\mu(\mathbf{x})$ with various σ_1; (b) curves of $\gamma(\mathbf{x})$ vs $\nu(\mathbf{x})$ with various σ_2; (c) curves of $\gamma(\mathbf{x})$ vs. $\kappa(\mathbf{x})$ with various σ_3; (d) curve of $\gamma(\mathbf{x})$ vs. μ, ν, κ with $\sigma_1=0.30$, $\sigma_2=0.25$, $\sigma_3=1.50$.

Then the LPA, consisting of luminance, chromatic and texture, is presented as follows.

1) *Luminance property*: since pixels located in thick hazy regions tend to have the highest intensities, an effective way is to evaluate the *luminance* at each pixel. Based on the *RGB* color channel information, this measure can be simply computed with the local mean of *RGB* color channels:

$$\mu(\mathbf{x}) = \frac{1}{3}\sum_{c\in\{r,g,b\}} \mathbf{I}_n^c(\mathbf{x}), \tag{6}$$

For hazy satellite image, the *luminance*-based measure performs as an identifier of dense and light haze regions. However, it cannot discriminate medium density haze regions from those with saturated colors. To overcome this problem, we consider two additional local properties.

2) *Chromatic property*: hazy satellite images generally present low saturation [14], and an effective way to measure this property is to evaluate the loss of colorfulness. Like the *luminance*-based measure, *chromatic*-based measure is also calculated based on *RGB* color channel information. It substitutes the local mean of *RGB* channels with the local deviation,

$$\upsilon(\mathbf{x}) = \sqrt{\frac{1}{3}\sum_{c\in\{r,g,b\}}\left[\mathbf{I}_n^c(\mathbf{x}) - \mu(\mathbf{x})\right]^2}, \tag{7}$$

Considering that $\mu(\mathbf{x})$ is calculated based on *RGB* channels, this measure will yield higher values in regions possessing saturated color. These regions are usually covered by light haze or even no haze at all. However, it is possible that this measure will assign small values not only for haze regions but also for those deteriorated due to some other reasons (e.g., *regions containing*

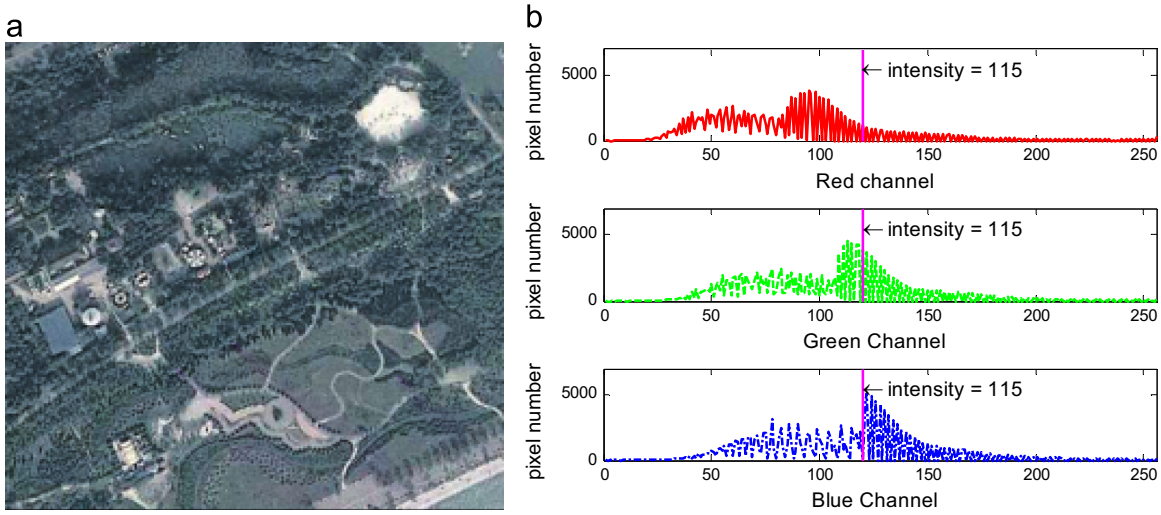

Fig. 6. Dehazing result of the image shown in Fig. 2 with our method: (a) dehazing result; (b) color intensity histograms for the enhanced image of each *RGB* channel. (For interpretation of the references to color in this figure legend, the reader is referred to the web version of this article).

light shadows, or areas vegetated with bushy trees). As a solution, we present the third property.

3) *Texture property*: Colorless regions can preserve more details than those covered by medium dense haze. An effective way is to characterize textural features. In this study, we extracted the *Sobel*-based local edge magnitude from intensity component of input image in *HSI* color space,

$$\kappa(\mathbf{x}) = \sqrt{\sum_{m=1}^{2} \left[\mathbf{I}^{(HSI)}(\mathbf{x}) \otimes w_s\right]^2}, \tag{8}$$

where, $\mathbf{I}^{(HSI)}$ is the normalized intensity component of hazy satellite image $\mathbf{I}$ in the *HSI* color space. w_s is the Sobel operator consisting of two pixel-wise and 3×3-sized convolution masks (horizontal and vertical) [26,27]. According to the definition above, small values are likely to be assigned to regions covered by medium density haze. While regions with plenty of detail, (e.g. *bushy trees*), will get higher values. Thus, this measure ensures that the possible haze regions can be well described.

By processing a large and diverse set of hazy satellite images, we can find that these three measures contribute almost the same. Therefore, we construct a normalized mixed exponential function (*NMEF*) $\gamma(\mathbf{x})$ depending on $\mu(\mathbf{x})$, $\upsilon(\mathbf{x})$ and $\kappa(\mathbf{x})$ to take their influences into account simultaneously.

$$\gamma(\mathbf{x}) = \exp\left[-\frac{(\mu(\mathbf{x})-\mu_{\max})^2}{2\sigma_1^2}\right]\cdot \exp\left[-\frac{(\upsilon(\mathbf{x})-\upsilon_{\min})^2}{2\sigma_2^2}\right]\cdot \left\{1-\exp\left[-\frac{(\kappa(\mathbf{x})-\kappa_{\max})^2}{2\sigma_3^2}\right]\right\}, \tag{9}$$

where $\mu_{\max}$, $\upsilon_{\min}$ and $\kappa_{\max}$ are the ideal values of $\mu(\mathbf{x})$, $\upsilon(\mathbf{x})$ and $\kappa(\mathbf{x})$. For the normalized hazy image, it is easy to respectively conclude that $\mu_{\max}=1$ and $\upsilon_{\min}=0$. While for $\kappa_{\max}$, Fig. 4 illustrates the flowchart by which it is calculated. σ_1, σ_2 and σ_3 are used to adjust the relative weights of $\mu(\mathbf{x})$, $\upsilon(\mathbf{x})$ and $\kappa(\mathbf{x})$.

Fig. 5(a)–(c) show the curves of $\gamma(\mathbf{x})$ vs. $\mu(\mathbf{x})$, $\upsilon(\mathbf{x})$ and $\kappa(\mathbf{x})$ with various σ_1, σ_2 and σ_3 respectively, while Fig. 5(d) is the curve of $\gamma(\mathbf{x})$ vs.$\mu(\mathbf{x})$, $\upsilon(\mathbf{x})$ and $\kappa(\mathbf{x})$ simultaneously.

As mentioned above, the coefficients σ_1, σ_2 and σ_3 are the parameters used for adjusting the influence of LPA on the *NMEF* respectively. It can be seen that if these parameters are set too bigger or too smaller than given values (or values in given range), significant truncated effects will occur for the curves of *NMEF*, which actually makes the *NMEF* curves degenerate to be piecewise linear ones. In the Section 2, we have demonstrated that it is not satisfying to dehaze the hazy satellite image only by simple linear model. However, the curves of *NMEF* with σ_1, σ_2 and σ_3 respectively set to 0.30, 0.25 and 1.50 are a good tradeoff. The actual *NMEF* possesses nice nonlinearity. It varies smoothly over the reasonable range of $\mu(\mathbf{x})$, $\upsilon(\mathbf{x})$ and $\kappa(\mathbf{x})$ when $\sigma_1=0.30$, $\sigma_2=0.25$ and $\sigma_3=1.50$. According to Fig. 5(d), $\gamma(\mathbf{x})$ begins to be active only when the haze density reaches a given value. For regions with very thin or no haze at all, the value of *NMEF* always nears zero, which means that the original *RGB* values are preserved. While for the regions with dense haze, a suitable value of *NMEF* is calculated based LPA, and then the original *RGB* values can be well restored.

Based on $\gamma(\mathbf{x})$, parameter $t(\mathbf{x})$ can be estimated as,

$$t(\mathbf{x}) = \max\left[1-\sin\left(\pi\gamma(\mathbf{x})/2\right), t_h\right], \tag{10}$$

where, t_h is a constant used to improve the robustness against noise during contrast enhancement when the haze is too dense. Then parameter $k(\mathbf{x})$ can be calculated as

$$k(\mathbf{x}) = 1/\max\left[1-\sin\left(\pi\gamma(\mathbf{x})/2\right), t_h\right], \tag{11}$$

3.2. Estimate parameter $b(\mathbf{x})$

Parameter $b(\mathbf{x})$ actually depends on $t(\mathbf{x})$ and $\mathbf{A}$. Since $t(\mathbf{x})$ is estimated as Eq. (10), the estimation of $b(\mathbf{x})$ can be converted to the estimation of $\mathbf{A}$. Considering that $\mathbf{A}$ originates from the effect of global atmospheric light in hazy satellite image degradation model, it is reasonable to determine $\mathbf{A}$ by the methods how to estimate atmospheric light.

He et al. [7] proposed a method based on DCP to estimate $\mathbf{A}$. They first pick up pixels among top 0.1% of brightness in the darkest channel, and then select the highest one as $\mathbf{A}$. Here, we adopt a modified version of He's method, which produces a similar result but performs more efficiently [9].

$$\mathbf{A} = \max_{(i,j)\in\Omega}\left\{\min_{w}{}_{(i,j)\in\Omega, c\in\{r,g,b\}}\left[\mathbf{I}^c(i,j)\right]\right\}, \tag{12}$$

where, Ω is the set of locations for all the pixels; $\min_w[\cdot]$ is the minimum filtering operation with a moving window w. This filter can reduce the risk of choosing the brightest ground target (or calling it a white ground target). According to Eq. (12), $\min_w[\cdot]$ is conducted on each channel of input image, and the maximum value of each color channel is then taken as the estimation of $\mathbf{A}$.

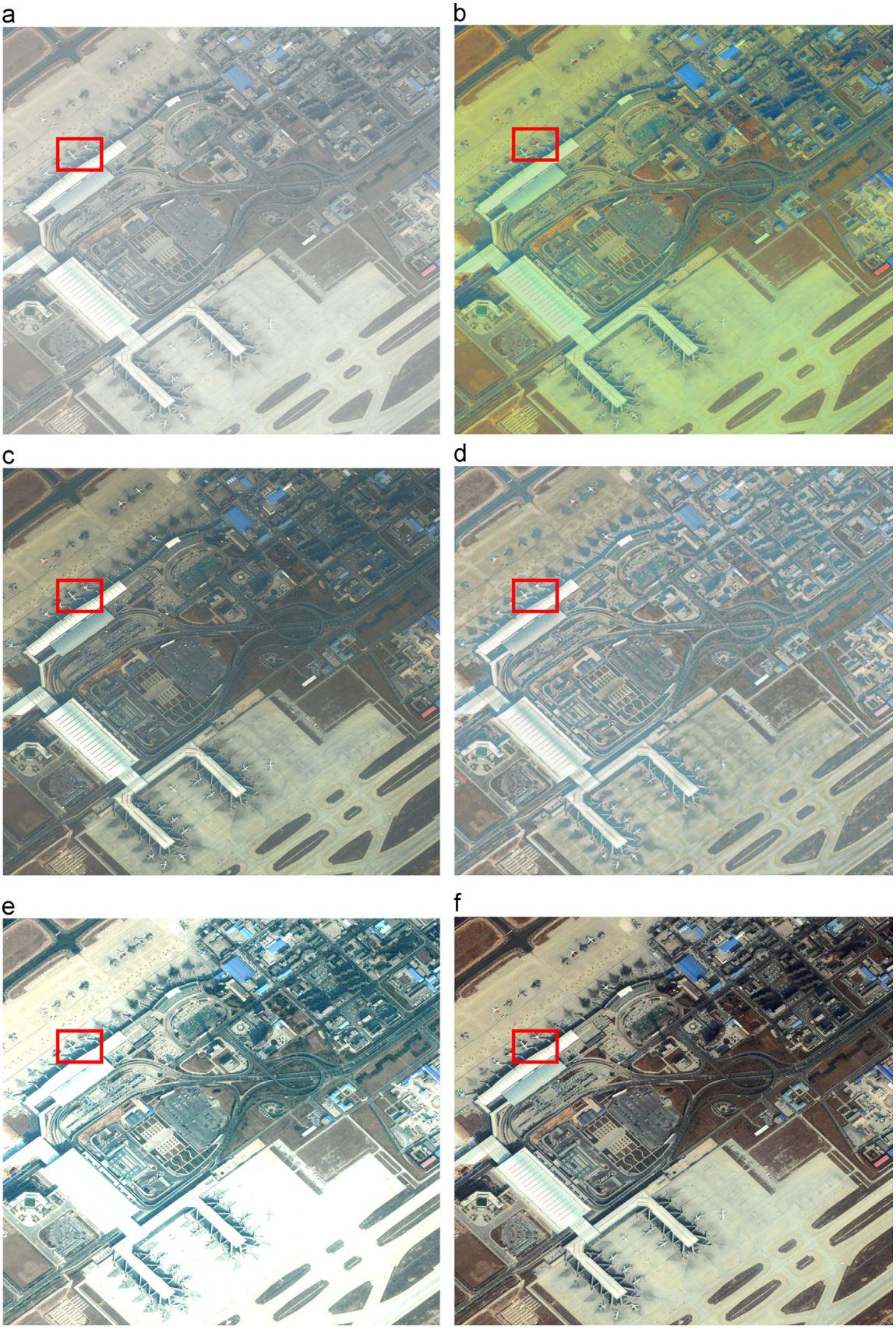

Fig. 7. From top to bottom and left to right, the original hazy satellite image and the results obtained by MSR, He et al. [16], Tarel [25], Fattal [14] and our method. (For interpretation of the references to color in this figure, the reader is referred to the web version of this article).

Then the parameter $b(\mathbf{x})$ of LIT can be estimated as:

$$b(\mathbf{x}) = \max_{(i,j)\in\Omega}\left\{\min_{w}{}_{(i,j)\in\Omega, c\in\{r,g,b\}}\left[\mathbf{I}^c(i,j)\right]\right\}\cdot\frac{1-\max\left[1-\sin\left(\pi\gamma(\mathbf{x})/2\right),t_h\right]}{\max\left[1-\sin\left(\pi\gamma(\mathbf{x})/2\right),t_h\right]} \tag{13}$$

Fig. 6 shows the final enhancement result of image in Fig. 2. Comparison with that in Fig. 3, the proposed method presents more brighter enhanced result, and the intensity histograms for three *RGB* channels become more uniformly distributed, tending to cover the entire density range from 0 to 255.

4. Experimental results

To evaluate the effectiveness of our method, in this section, we present the experiment results with hazy satellite images, which are collected from *Google Earth* and *NASA Earth Observatory website*. These images differ with scene content, spatial resolution and haze density, and are respectively used for different applications. We compare the performance of our method both qualitatively and quantitatively with multiple scale Retinex (noted as MSR), and several state-of-the-art approaches, including He et al.'s [16], Tarel's [25] and Fattal's [14].

Except special illustration, the local window w_s of *Sobel* edge operators is sized by 3×3 [28] [29]. The coefficients σ_1, σ_2 and σ_3 are respectively set to 0.30, 0.25 and 1.50. As for the methods to be compared, we set the key parameters as the corresponding papers. We implemented our method with Matlab 2013 on a Windows 7 PC with an Intel(R) Core(TM) 2 CPU 6320 @ 1.86 GHz processor.

4.1. Qualitative evaluation

Fig. 7 presents experimental results for a hazy satellite image of *Xianyang International Airport* downloaded from *Google Earth*. The image size of 1500×1500, and its spatial resolution is about 0.50 m. In this scene, there are quite a number of different types of ground targets, e.g. *houses, cars, roads, runways and planes*. It can be seen that, our method provides the best dehazing result with rich details and abundant color information, which are both of great importance for human visual perception and further image analysis. In contrast, the results of the other methods are not so quite satisfying. For example, as a typical method based on multiplicative imaging model, Retinex darkens the image after dehazing, and the color of most regions have also been significantly disturbed. The existence of large-scale white targets instead of the shy makes the estimation of *airlight***A**in He et al.'s method [16] questionable. The image dehazed by this method is overall darkened even that the haze is removed more or less. Particularly, the local details in shadow regions are very difficult to interpret. Tarel's [25] method dehazes this image not so quite visually compelling with halo appearing in the regions where sharp change of luminance (e.g. *shadows*) occurs. Considering that the gray effect of haze makes the assumption of enough color information does not hold, Fattal's method [14] over-brightens the hazy image and present abnormal colors.

To further illustrate the outstanding performance of our method over the other four methods, we take some local patches from the images in Fig. 7, and present them in Fig. 8. Obviously, the patch dehazed by our method has best contrast and color preservation. For instance, the boundaries of shadow regions are more vivid than those taken from the images dehazed by the other four methods.

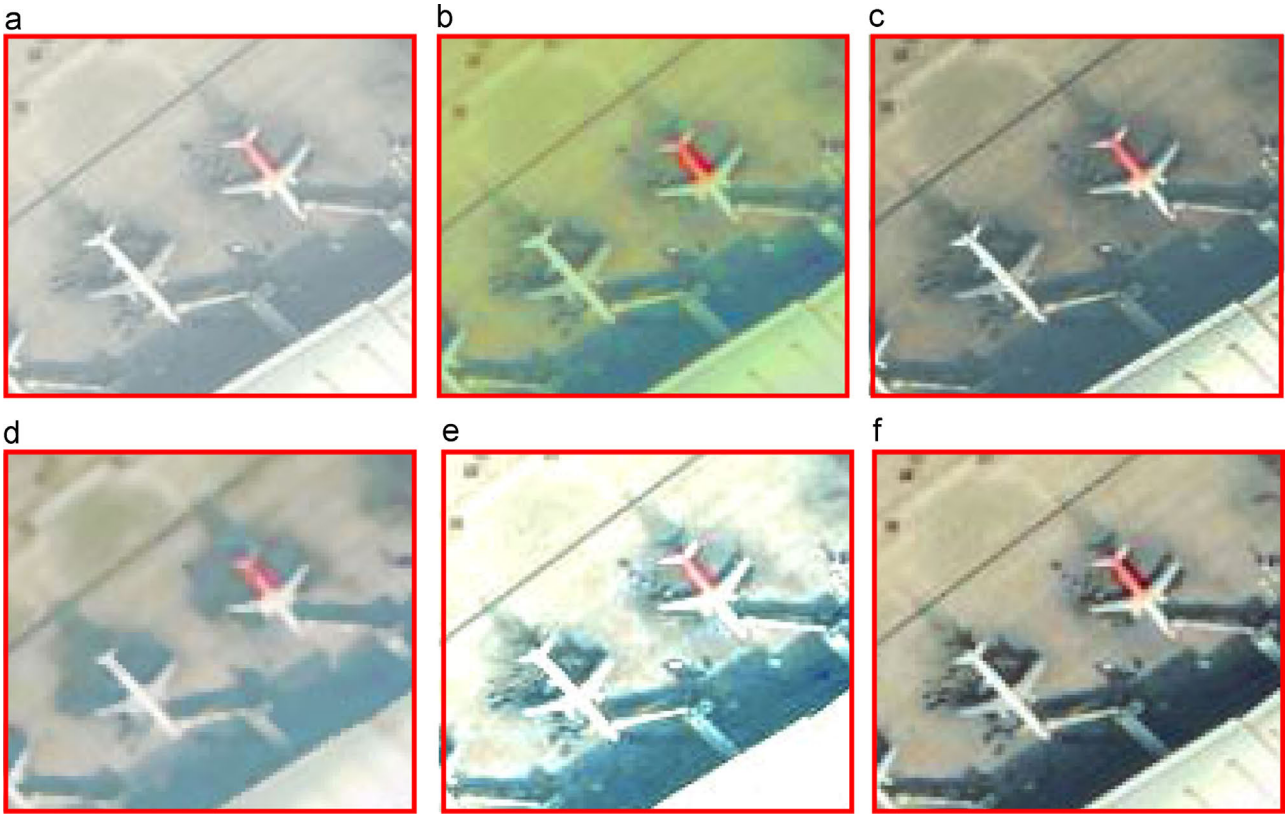

Fig. 8. Local patches taken for detailed visual comparison. From top to bottom and left to right, the original hazy satellite image and the results obtained by MSR, He et al. [16], Tarel [25], Fattal [14] and our method. (For interpretation of the references to color in this figure, the reader is referred to the web version of this article).

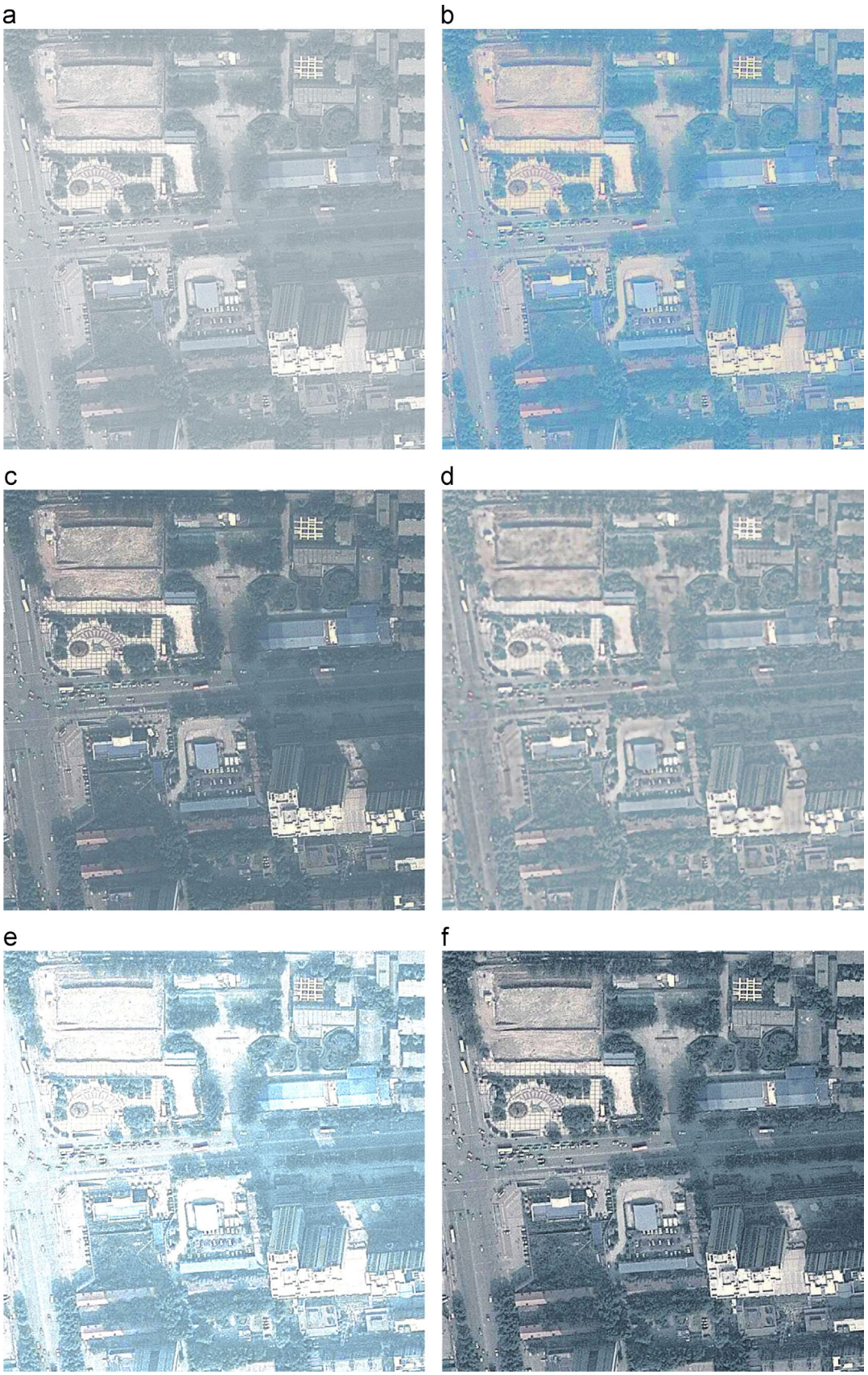

Fig. 9. From top to bottom and left to right, the original hazy satellite image and the results obtained by MSR, He et al.'s [16], Tarel's [25] and Fattal's [14] and our method. (For interpretation of the references to color in this figure, the reader is referred to the web version of this article).

Fig. 10. From top to bottom and left to right, the original hazy satellite image and the results obtained by MSR, He et al.'s [16], Tarel's [25] and Fattal's [14] and our method. (For interpretation of the references to color in this figure, the reader is referred to the web version of this article).

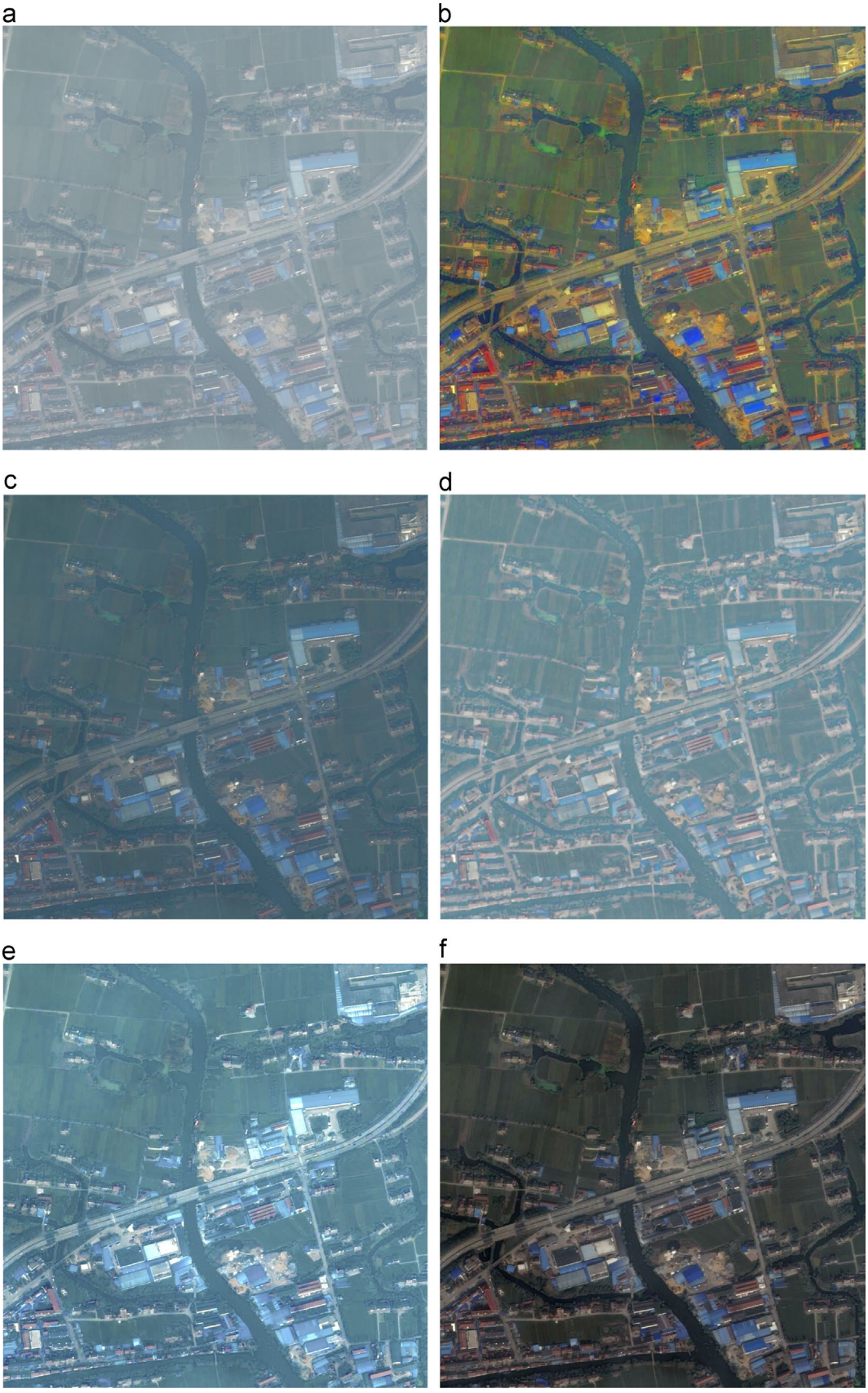

Fig. 11. From top to bottom and left to right, the original hazy satellite image and the results obtained by MSR, He et al.'s [16], Tarel's [25] and Fattal's [14] and our method.

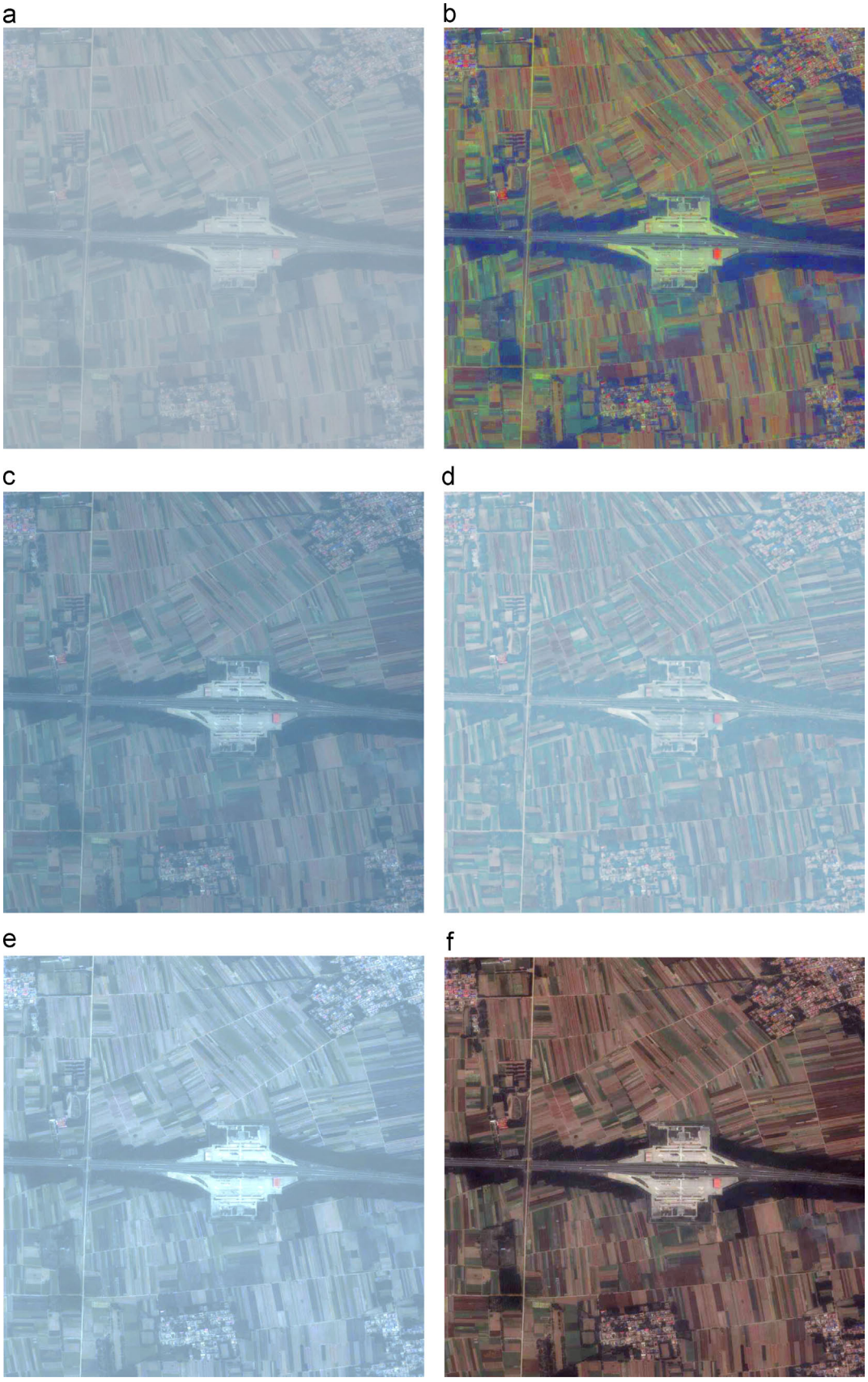

Fig. 12. From top to bottom and left to right, the original hazy satellite image and the results obtained by MSR, He et al.'s [16], Tarel's [25] and Fattal's [14] and our method. (For interpretation of the references to color in this figure, the reader is referred to the web version of this article).

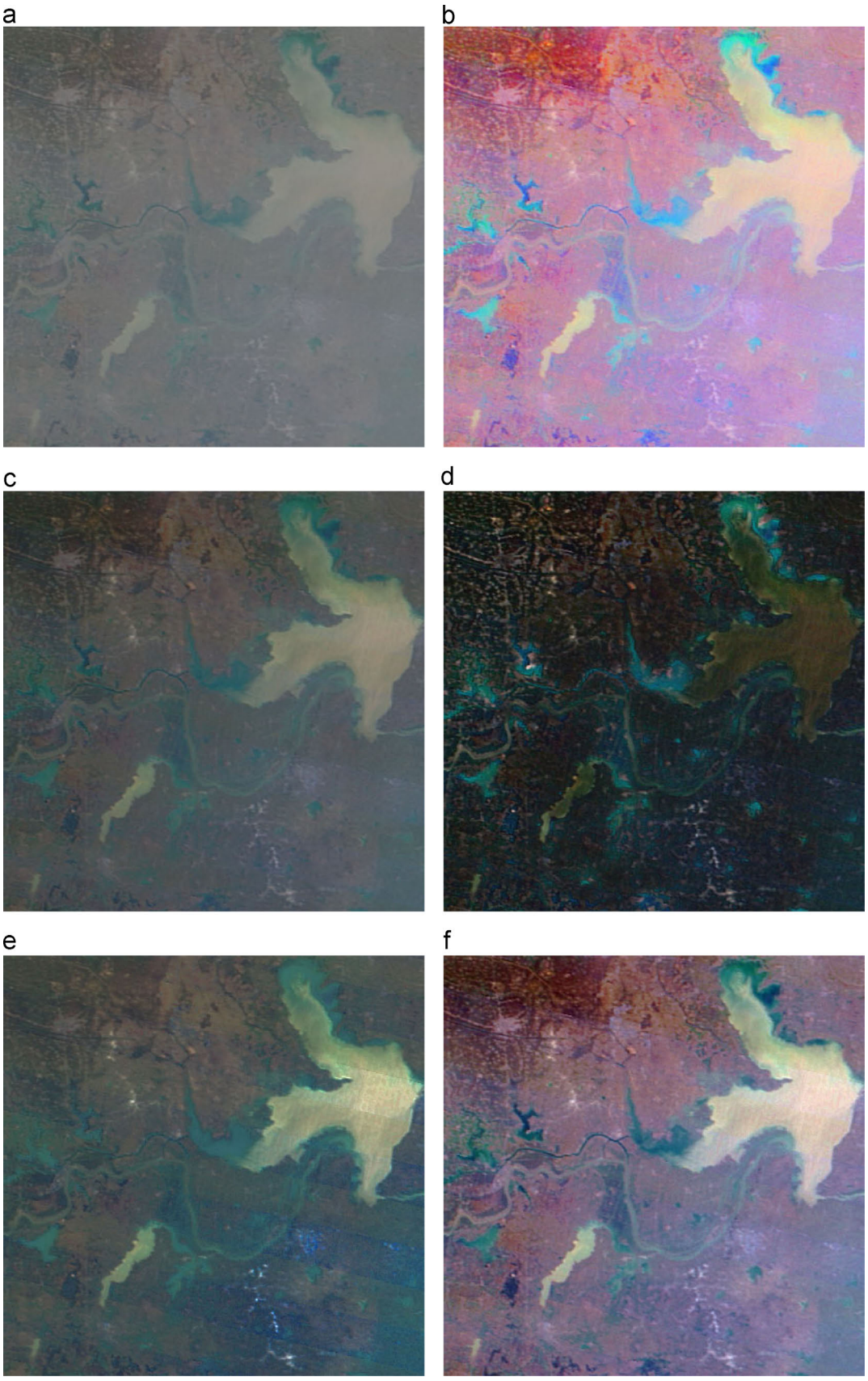

Fig. 13. From top to bottom and left to right, the original hazy satellite image and the results obtained by MSR, He et al.'s [16], Tarel's [25] and Fattal's [14] and our method. (For interpretation of the references to color in this figure, the reader is referred to the web version of this article).

In Figs. 9 and 10, we evaluate the performance of our method and the other four methods with hazy satellite images obtained over city scenes downloaded from *Google Earth*. In Fig. 9, the image size is 600×600, and its spatial resolution is about 0.50 m. This image contains several tall buildings associated with their significant shadows, many vehicles moving on the roads, and dark green trees. Due to the overall relative dense haze, this image looks very blurring. In Fig. 10, the image size is 1500×1500, and its spatial resolution is about 1.00 m. This image contains many house buildings, a concrete square and large water area of a river. It can be seen that our method can well avoid the problem of excessive color saturation and distortion. The details are presented clearly. Even the local contrast of the region under tall buildings' shadows has been enhanced. However, the results obtained by the other four methods still suffer from the problems of luminance darkened, color disturbed. For example, Fattal's method [14] resulted in excessively saturated color, especially in Fig. 9(b).

In Figs. 11 and12, we evaluate the performance of our method and the other four methods with hazy satellite images obtained over urban regions downloaded from *Google Earth*. In Fig. 11, the image size is 1600×1500, and its spatial resolution is about 1.00 m. This image contains farmlands, dispersed houses, and rivers. In Fig. 12, the image size is 1000×1000, and its spatial resolution is about 10.00 m. This image mainly contains farmlands and several hamlets. Compared with the high reflection of airlight by buildings in city regions, the relative low reflectivity of farmlands causes such images looks deep-colored. For such images, our method can also obtain satisfying result. However, the actual relative low reflection of airlight destroys the corresponding assumption of He et al.'s [16], Tarel's [25] and Fattal's [14] methods. Thus, the results obtained by such three methods look hazy. While for MSR, it over-dehazed these images with saturated color in local regions.

In Fig. 13, our method and the other four methods were evaluated with a hazy satellite image downloaded from *NASA Earth Observatory website*. This image size is 400×400, and its spatial resolution is about 250 m. It contains the Hongze Lake in Jiangsu province of China. Due to the dense and dusty haze, the color of this image is overall dark except the region of Hongze Lake. We can see that the dehazing result by MSR method suffers significantly red-shifted and locally color saturation. Because the dense and dusty haze also makes the airlight questionable, the dehazing results obtained by He et al.'s [16], Tarel's [27] and Fattal's [14] are all darkened, making some local details hard to interpret. However, the result by our method looks much more vivid.

4.2. Quantitative evaluation

Four objective indicators are employed to assess the corresponding results quantitatively, among which three ones, e, $\bar{r}$, and p, are defined as [28], and the forth one, τ ,, is noted as the time consuming. Indicator e represents the rate of edges newly visible after enhancement. Indicator $\bar{r}$ measures how much the contrast between the background and the target is enhanced. Finally, to evaluate the level of oversaturation, indicator p is introduced as the percentage of pixels being completely white or black in the restored image. A better dehazed image is generally supposed to have higher values of e and$\bar{r}$, and lower values of p andτ . The results are list in Table 1.

It is observed from these tables that our method performs well for all these four indicators, especially for e, which means the dehazed image presents more local details. In addition, for given hazy satellite image, the time consuming of our method is less than 10 times than that of Fattal's method [14]. However, the other three indicators of Fattal's method [14] are not quite promising. As for He et al.'s method [16], the questionable *airlight* estimation and the abundant local details makes the soft-matting based transmission estimation quite time consuming.

Table 1
Quantitative evaluation results.

Indicator	Method	e	$\bar{r}$	p (%)	τ (s)
Fig. 7	Original (a)	–	–	–	
	MSR (b)	0.3901	1.1878	**0**	10.2147
	He et al.'s (c)	0.4136	1.1895	0.1622	2.41×10^6
	Tarel's (d)	0.2638	1.4413	0.0311	643.2988
	Fattal's (e)	0.6432	**2.5858**	20.3795	**1.3605**
	Ours (f)	**0.7936**	2.3009	0.0508	6.6648
Fig. 9	Original (a)	–	–	–	
	MSR (b)	0.3250	1.1500	**0**	2.5874
	He et al.'s (c)	0.6983	1.3493	0.0148	4.73×10^5
	Tarel's (d)	0.2428	1.3301	0.2639	61.3782
	Fattal's (e)	0.8048	2.2727	8.9838	**0.1956**
	Ours (f)	**0.9080**	**2.4856**	0.1195	1.2539
Fig. 10	Original (a)	–	–	–	
	MSR (b)	1.1911	1.3091	**0**	8.5134
	He et al.'s (c)	0.6472	0.9489	**0**	2.29×10^6
	Tarel's (d)	0.9810	**2.1423**	**0**	627.1398
	Fattal's (e)	0.8944	1.6894	0.1970	**1.0937**
	Ours (f)	**2.1489**	1.6048	**0**	6.7841
Fig. 11	Original (a)	–	–	–	
	MSR (b)	4.5951	1.9671	**0**	15.1605
	He et al.'s (c)	1.5065	1.0347	0.0034	3.85×10^6
	Tarel's (d)	1.0621	1.6668	0.0032	733.4166
	Fattal's (e)	3.9640	**2.4473**	0.1877	**1.3270**
	Ours (f)	**8.1846**	1.9508	0.0038	6.6238
Fig. 12	Original (a)	–	–	–	
	MSR (b)	50.1761	3.0402	**0**	7.6281
	He et al.'s (c)	10.6391	1.7343	**0**	2.66×10^4
	Tarel's (d)	9.2983	2.0994	**0**	160.9419
	Fattal's (e)	13.0522	2.4777	0.0096	**0.5498**
	Ours (f)	**70.3180**	**3.7112**	**0**	2.8078
Fig. 13	Original (a)	–	–	–	
	MSR (b)	1.4793	2.2529	**0**	0.8018
	He et al.'s (c)	2.0753	1.2511	**0**	1.59×10^5
	Tarel's (d)	**9.9084**	**2.8993**	**0**	39.5493
	Fattal's (e)	5.7267	1.9701	**0**	**0.1032**
	Ours (f)	4.2289	2.6134	**0**	0.7901

Fig. 14 shows result of our method conducted on very dense hazy satellite image. As we can see, the local details and color information can also be roughly recovered. In addition, Fig. 15 indicates that our method can obtain comparable performance on outdoor images. So the LPA may have some potential to describe image depth that is related with haze variations.

In conclusion, due to the good suitability of LIT model in describing the degradation of hazy remote sensing, and the effectiveness and efficiency of LPA based parameter estimation, our method outperforms than the dehazing methods compared.

5. Conclusion and future work

In this paper, we have proposed a simple but effective method to remove the haze from single satellite image. This method is developed based on the LIT and LPA. We demonstrate that it is reasonable to use LIT to enhance the visibility of hazy satellite imagery. Then, we propose to adaptively estimate parameters of LIT by analyzing the local image properties of luminance, chromatics and texture. Experimental results on hazy satellite images indicate that our method outperforms four well-known dehazing methods, including both classical and state-of-the-arts.

In the future, there are at least two problems worth of further study, one is how to construct more suitable statistics to discriminate thick haze and large-scale white ground targets more

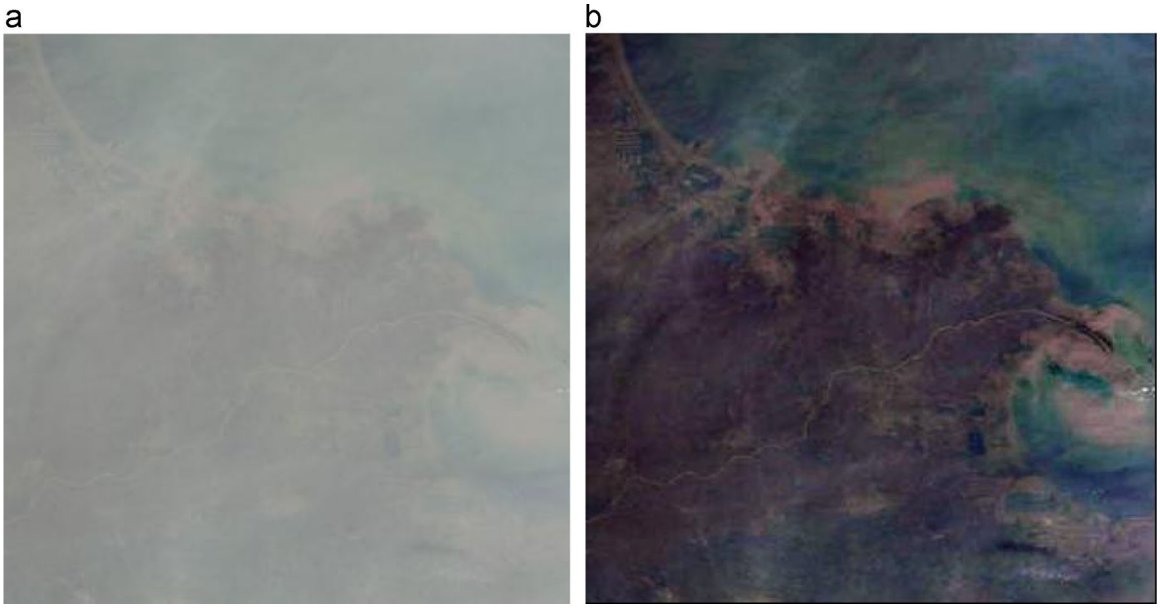

Fig. 14. Results by our method for satellite image with very dense haze. (a) Original image. (b) Dehazing result. (For interpretation of the references to color in this figure, the reader is referred to the web version of this article).

Fig. 15. From left to right and top to bottom, the input hazy outdoor image and the results obtained by MSR, He et al.'s [16], Tarel's [25] and Fattal's [14] and our method. (For interpretation of the references to color in this figure, the reader is referred to the web version of this article).

efficiently, and the other one is how to find the most optimized values for the coefficients used in *NMEF*.

Acknowledgments

This work was supported in part by the National Natural Science Foundation of China (Grant nos. 61125204 and 61432014), the Fundamental Research Funds for the Central Universities (Grant nos. K5051202048 and BDZ021403), Microsoft Research Asia Project based Funding (Grant no. FY13-RES-OPP-034), the Program for Changjiang Scholars and Innovative Research Team in University of China (No. IRT13088) and the Shaanxi Innovative Research Team for Key Science and Technology (No. 2012KCT-02).

References

[1] J. Benediktsson, J. Chanussot, W. Moon, Advances in very high resolution remote sensing, Proc. IEEE 101 (3) (2013) 566–569.
[2] G. Cheng, et al., Multi-class geospatial object detection and geographic image classification based on collection of part detectors, ISPRS J. Photogramm. Remote Sens. 98 (2014) 119–132.
[3] A. Berjon, V. Cachorro, P. Zarco, A. Frutos, Retrieval of biophysical vegetation parameters using simultaneous inversion of high resolution remote sensing imagery constrained by a vegetation index, Precis. Agric. 14 (2013) 541–557.
[4] X. Huang, H. Liu, L. Zhang, Spatiotemporal detection and analysis of urban villages in mega city regions of China using high-resolution remotely sense, IEEE Trans. Geosci. Remote Sens. 53 (7) (2015) 3639–3657.
[5] G. Cheng, et al., Automatic landslide detection from remote-sensing imagery using a scene classification based on BoVW and pLSA, Int. J. Remote Sens. 34 (1) (2013) 45–59.
[6] G. Cheng, et al., Object detection in remote sensing imagery using a discriminatively trained mixture model, ISPRS J. Photogramm. Remote Sens. 85 (2013) 32–43.
[7] Y. Xiong, H. Yan, C. Yu, Algorithm of removing thin cloud-fog cover from single remote sensing image, J. Inf. Comput. Sci. 11 (3) (2014) 817–824.
[8] T. Arici, S. Dikbas, Y. Altunbasak, A histogram modification framework and its application for image contrast enhancement, IEEE Trans. Image Process. 18 (9) (2009) 1921–1935.
[9] Z. Zhou, N. Sang, X. Hu, Global brightness and local contrast adaptive enhancement for low illumination color image, Optik 125 (2014) 1795–1799.
[10] S. Lee, An efficient content-based image enhancement in the compressed domain using retinex theory, IEEE Trans. Circuits Syst. Video Technol. 17 (2) (2007) 199–213.
[11] G.D. Moro, L. Halounova, Haze removal for high-resolution satellite data: a case study, Int. J. Remote Sens. 28 (10) (2007) 2187–2205.
[12] Y. Schechner, S. Narasimhan, S. Nayar, Instant dehazing of images using polarization, in: Proceedings of the IEEE Conference on Computer Vision and Pattern Recognition, CVPR 2001, IEEE, Anchorage, AK, USA, 1 (2008), pp. 325–332.
[13] S. Shwartzet al., Blind haze separation, in: Proceedings of the IEEE Conference on Computer Vision and Pattern Recognition, CVPR 2001, IEEE, Anchorage, AK, USA, (2006), pp. 1984–1991.
[14] R. Fattal, Single image dehazing, ACM Trans. Graph. 27 (3) (2008) 1–9.
[15] R.T. Tan, Visibility in bad weather from a single image, in: Proceedings of the IEEE Conference on Computer Vision and Pattern Recognition, 2008, CVPR 2008, IEEE, Anchorage, AK, USA, (2008), pp. 1–8.
[16] K. He, J. Sun, X. Tang, Single image haze removal using dark channel prior, IEEE Trans. Pattern Anal. Mach. Intell. 33 (12) (2010) 2341–2353.
[17] G. Meng, Y. Wang, J. Duan, S. Xiang, and C. Pan, Efficient image dehazing with boundary constraint and contextual regularization, in: Proceedings IEEE Conference on Computer Vision and Pattern Recognition, CVPR 2013, 2013, pp. 617–624.
[18] J. Wang, N. He, L. Zhang, K. Lu, Single image dehazing with a physical model and dark channel prior, Neurocomputing 149 (2015) 718–728.
[19] J. Li, H. Zhang, D. Yuan, M. Sun, Single image dehazing using the change of detail prior, Neurocomputing 156 (2015) 1–11.
[20] J. Long, Z. Shi, W. Tang, C. Zhang, Single remote sensing image dehazing, IEEE Geosci. Remote Sens. Lett. 11 (1) (2014) 59–63.
[21] Y. Lai, Y. Chen, C. Chiou, C. Hsu, Single image dehazing via optimal transmission map under scene priors, IEEE Trans. Circuits Syst. Video Technol. 25 (1) (2015) 1–14.
[22] A. Loza, D. Bull, and A. Achim, Automatic contrast enhancement of low-light images based on local statistics of wavelet coefficients, in: Proceedings of the IEEE Conference on Image Processing, ICIP 2011, 2011, pp. 3553–3556.
[23] K. Huang, Z. Wu, Q. Wang, Image enhancement based on the statistics of visual representation, Image Vis. Comput. 23 (1) (2005) 51–57.
[24] E. Lee, S. Kim, W. Kang, D. Seo, J. Paik, Contrast enhancement using dominant brightness level analysis and adaptive intensity transformation for remote sensing images, IEEE Geosci. Remote Sens. Lett. 10 (1) (2013) 62–66.
[25] J. Tarel, N. Hautiere, L. Caraffa, A. Cord, H. Halmaoui, D. Gruyer, Vision, enhancement in homogeneous and heterogeneous fog, IEEE Intell. Transp. Syst. Mag. 4 (2) (2012) 6–20.
[26] I. Sobel, An Isotropic 3×3 Gradient Operator, Machine Vision for Three – Dimensional Scenes, H. Freeman, Academic Pres, NY (1990), p. 376–379.
[27] R.C. Gonzalez, R.E. Woods, Digital Image Processing, 2nd ed., Prentice Hall, Inc., USA (2002), p. 567–612.
[28] N. Hautiere, J.-P. Tarel, D. Aubert, E. Dumont, et al., Blind contrast enhancement assessment by gradient ratioing at visible edges, Image Anal. Stereol. J 27 (2) (2008) 87–95.

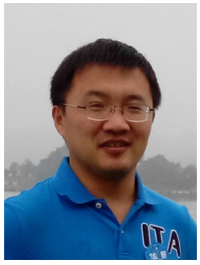

Weiping Ni received the B.S. degree in electronic science and technology from University of Science and Technology of China, Hefei, China, in 2004 and the M.S. 1degree in signal processing from National University of Defense Technology, Changsha, China, in 2006. He is currently pursuing the Ph.D. degree in pattern recognition and intelligent system at Xidian University, Xi'an, China. From 2014 to now, he has been a Research Associate with the Northwest Institute of Nuclear Technology, Xi'an, China. His research interest includes remote sensing image processing, automatic target recognition, and computer vision.

Xinbo Gao (M'02-SM'07) received the B.Eng., M.Sc., and Ph.D. degrees in signal and information processing from Xidian University, Xi'an, China, in 1994, 1997, and 1999, respectively. From 1997 to 1998, he was a Research Fellow at the Department of Computer Science, Shizuoka University, Shizuoka, Japan. From 2000 to 2001, he was a Post-Doctoral Research Fellow at the Department of Information Engineering, the Chinese University of Hong Kong, Hong Kong. Since 2001, he has been at the School of Electronic Engineering, Xidian University. He is currently a Cheung Kong Professor of Ministry of Education, a Professor of Pattern Recognition and Intelligent System, and the Director of the State Key Laboratory of Integrated Services Networks, Xi'an, China. His current research interests include multimedia analysis, computer vision, pattern recognition, machine learning, and wireless communications. He has published five books and around 200 technical articles in refereed journals and proceedings. Prof. Gao is on the Editorial Boards of several journals, including Signal Processing (Elsevier), and Neurocomputing (Elsevier). He served as the General Chair/Co-Chair, Program Committee Chair/Co-Chair, or PC Member for around 30 major international conferences. He is currently a fellow of the Institution of Engineering and Technology.

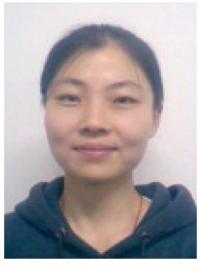

Ying Wang received the B.Sc., M.Sc. and doctor degrees in signal and information processing from the Xidian University, Xi'an, China, in 2003, 2006, and 2010 respectively. She is now an associate professor of Signal and Information Processing in Xidian University. Her research interests include medical image analysis, pattern recognition and computer-aided diagnosis.